Supporting Information

Mechanistic Investigation on the Polymerization of Phenylacetylene by 2-Diphenylphosphinopyridine Rhodium(I) Catalysts: Understanding the Role of the Cocatalyst and Alkynyl Intermediates

Marta Angoy, M. Victoria Jiménez, F. Javier Modrego, Luis A. Oro, Vincenzo Passarelli, and Jesús J. Pérez-Torrente

Departamento de Química Inorgánica, Instituto de Síntesis Química y Catálisis Homogénea–ISQCH, Universidad de Zaragoza–CSIC, Facultad de Ciencias, C/ Pedro Cerbuna, 12, 50009 Zaragoza, Spain; and Centro Universitario de la Defensa, Ctra. Huesca s/n, ES−50090 Zaragoza, Spain

1.- NMR spectra of 2-diphenylphosphinopyridine rhodium(I) compounds.

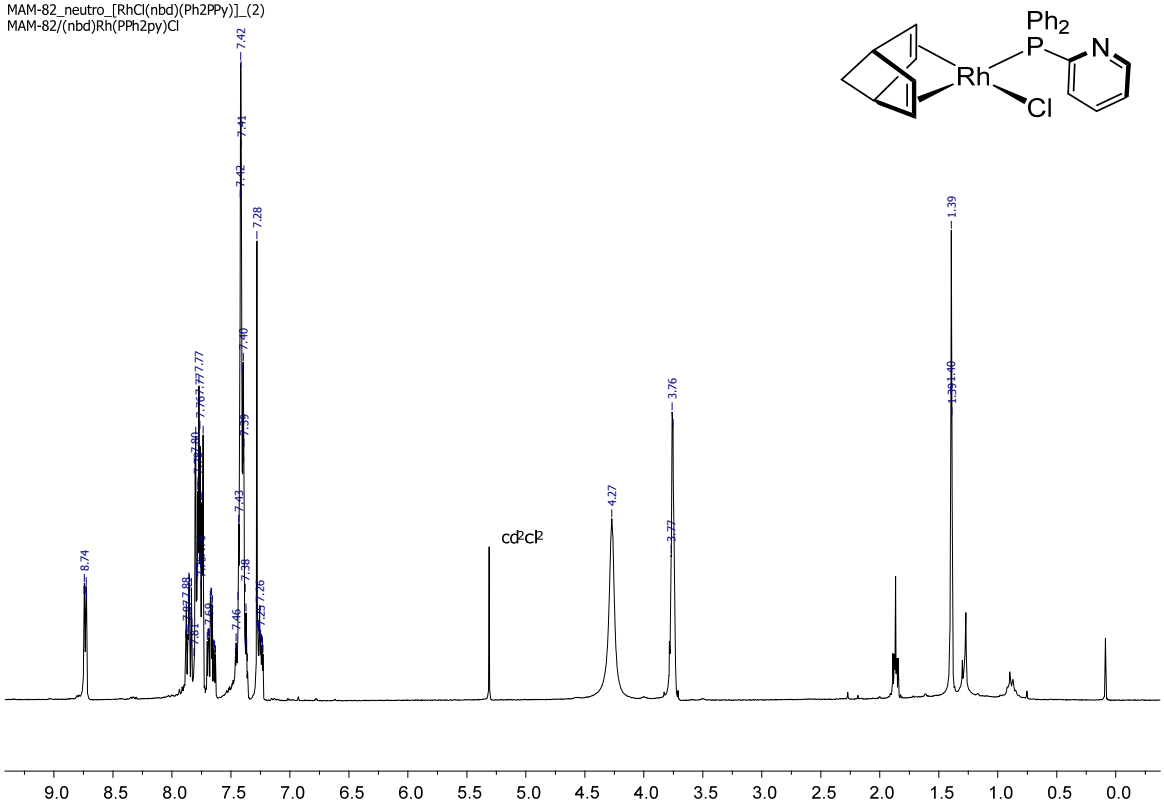

Figure S1. ^{1}H NMR spectra of compound [RhCl(nbd)(Ph_2PPy)] (**2**) in CD_2Cl_2 at 298K.

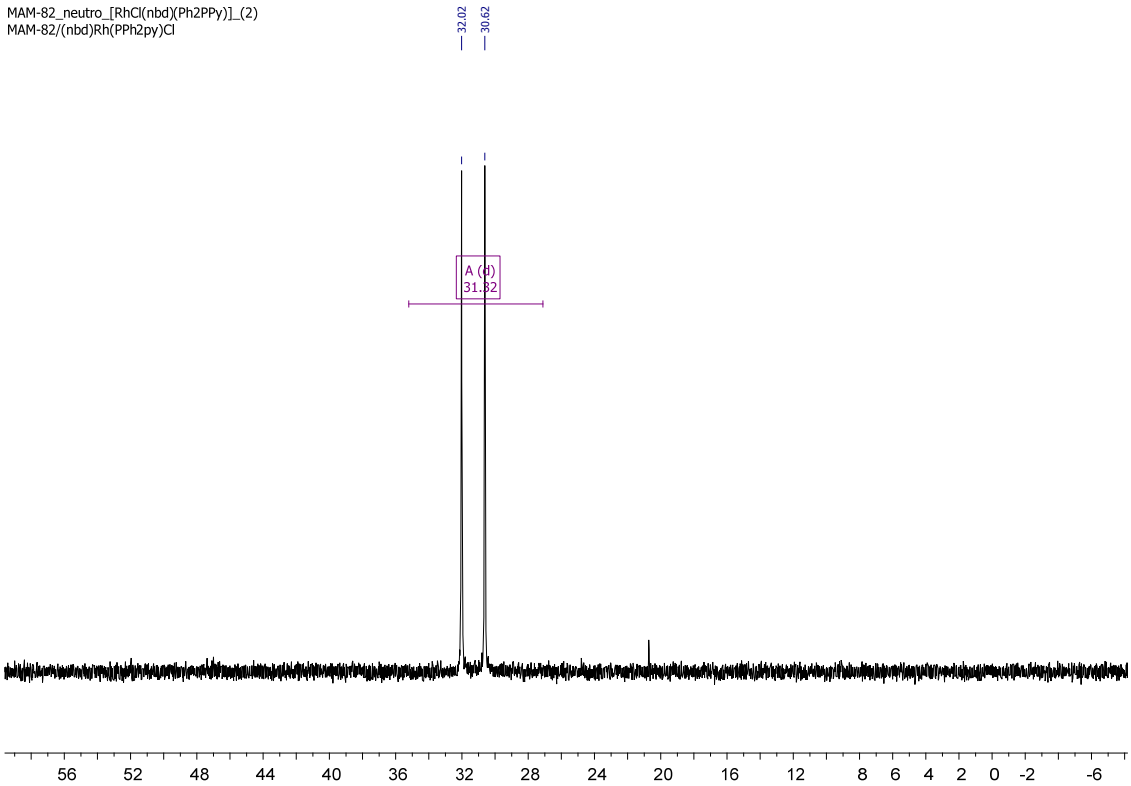

Figure S2. ^{31}P{^{1}H} NMR spectra of compound [RhCl(nbd)(Ph_2PPy)] (**2**) in CD_2Cl_2 at 298K.

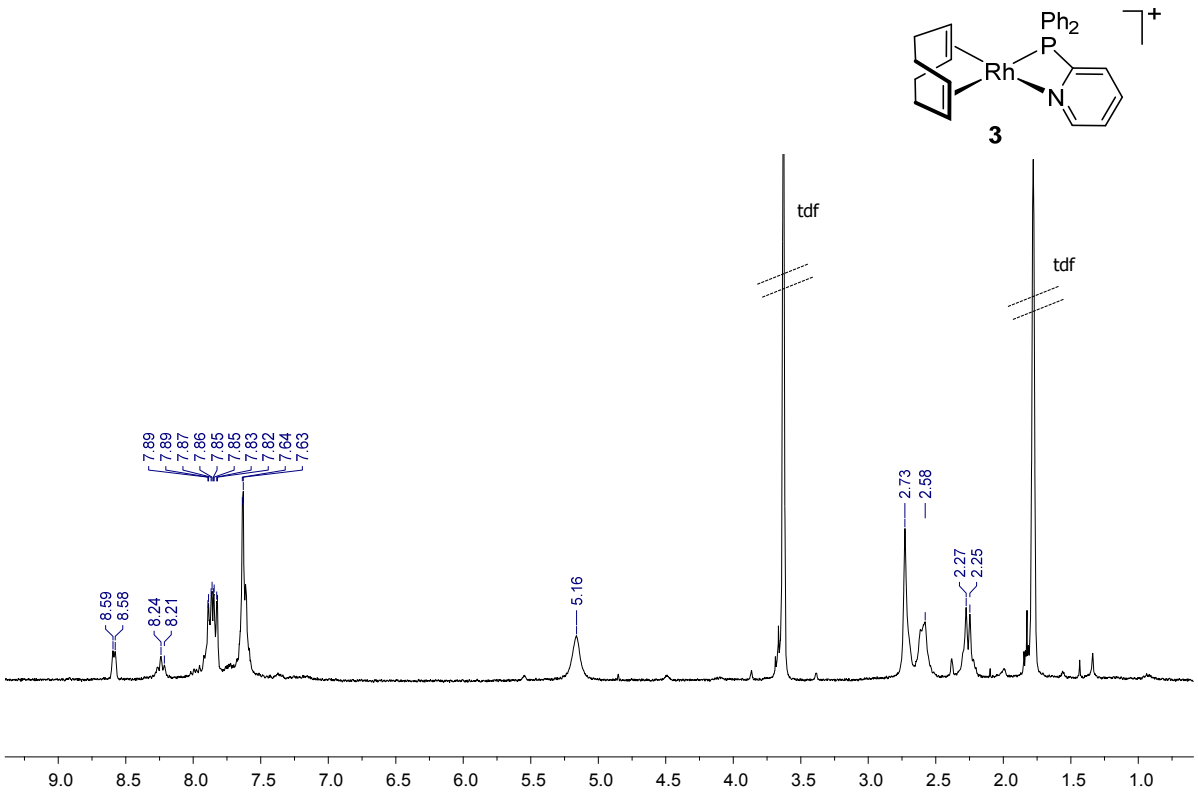

Figure S3. ^{1}H NMR spectrum of compound [Rh(cod)(Ph_2PPy)][BF_4] (**3**) (THF-d_8, 273 K)

a)

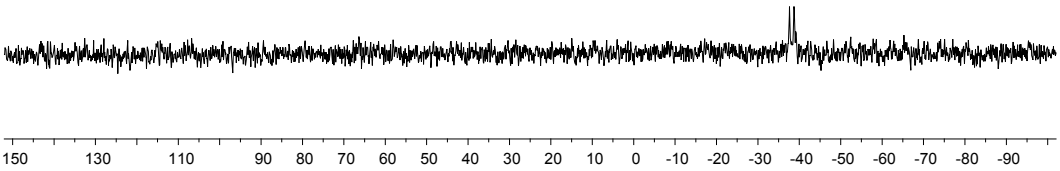

b)

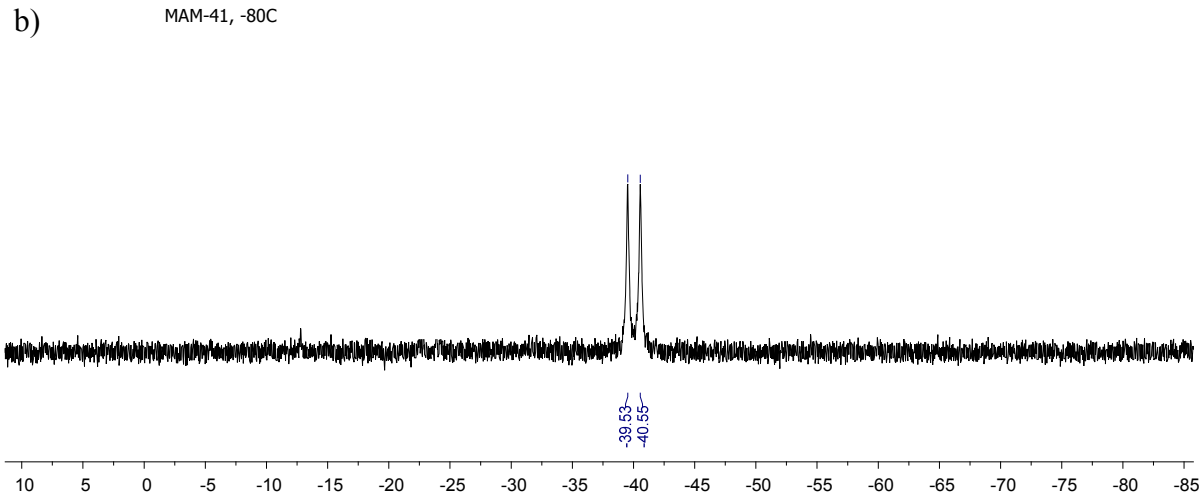

Figure S4. ^{31}P{^{1}H} NMR spectra of compound [Rh(cod)(Ph_2PPy)][BF_4] (**3**) in THF-d_8: a) 273 K, b) 193 K.

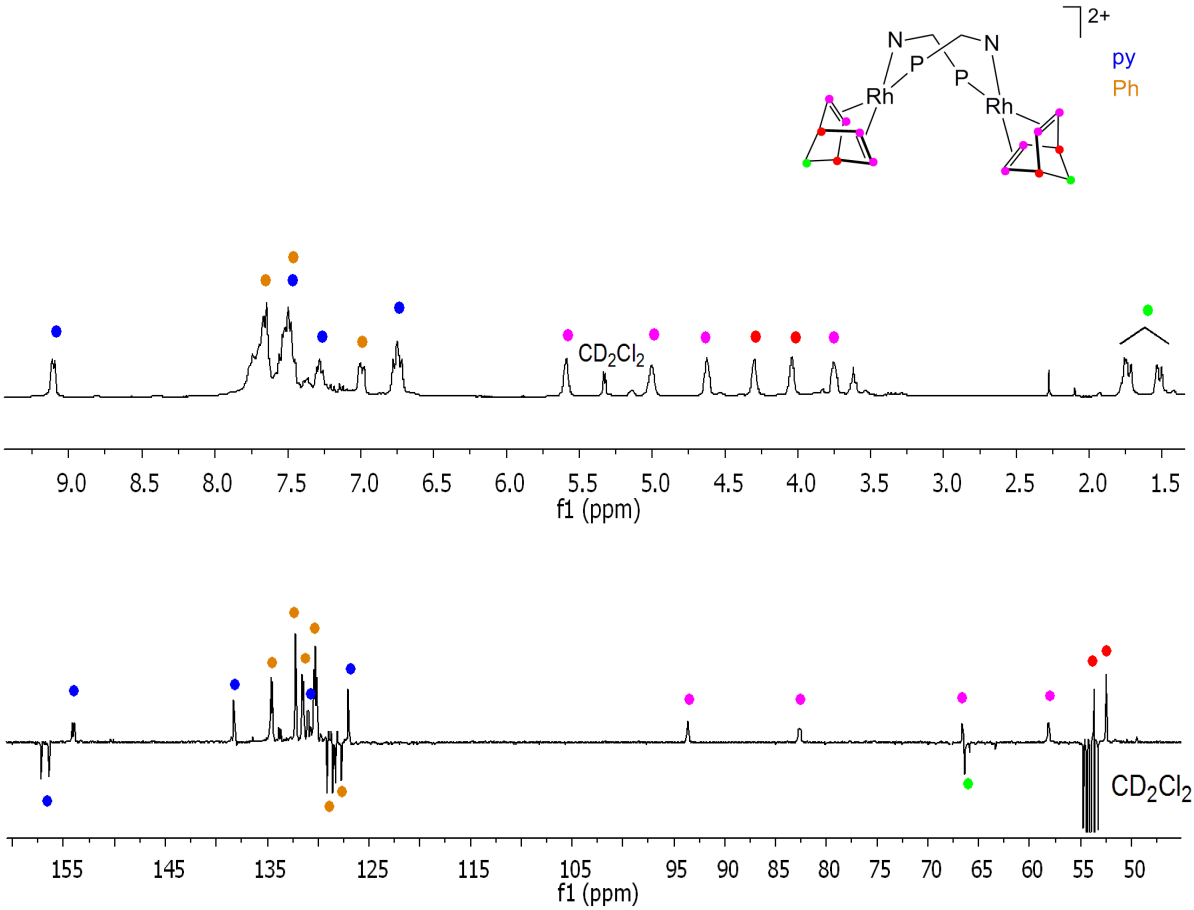

Figure S5. ^{1}H and ^{13}C{^{1}H}-apt NMR spectra of compound [Rh(nbd)(μ-Ph_2PPy)]$_2$[BF_4]$_2$ (**4**) in CD_2Cl_2 at 233K.

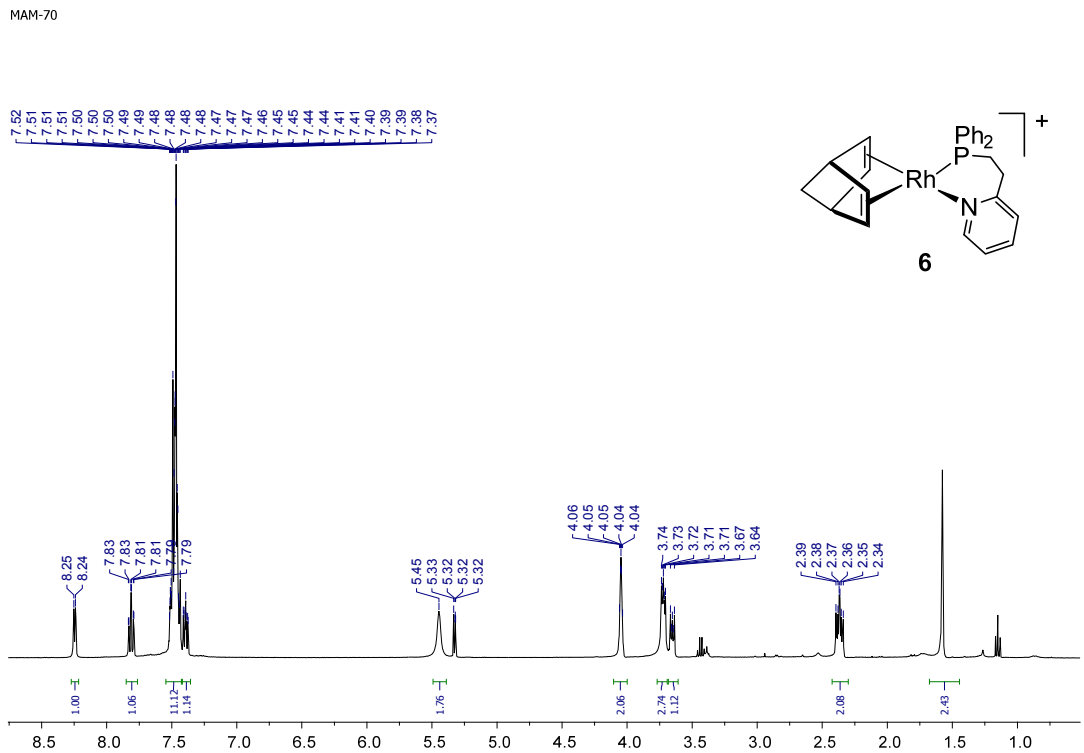

Figure S6. ^{1}H NMR spectra of compound [Rh(nbd){$Ph_2(CH_2)_2Py$}]BF_4 (**6**) in CD_2Cl_2 at 298K.

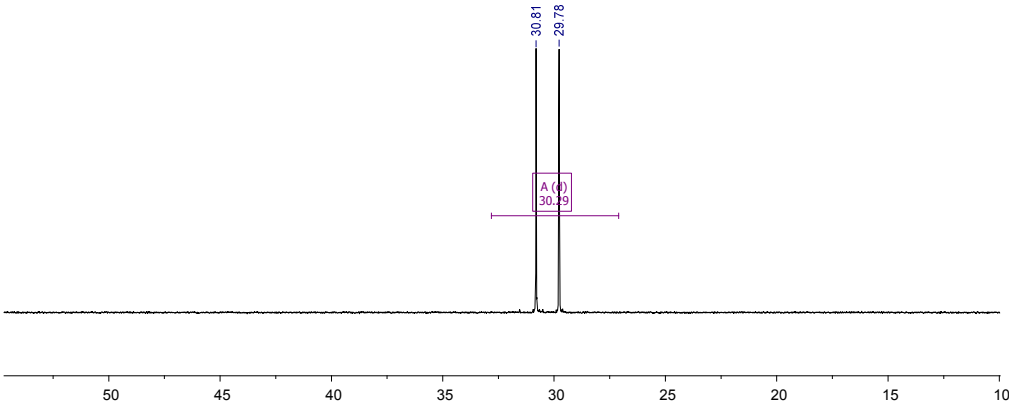

Figure S7. $^{31}P\{^{1}H\}$ NMR spectra of compound $[Rh(nbd)\{Ph_2(CH_2)_2Py\}]BF_4$ (**6**) in CD_2Cl_2 at 298K.

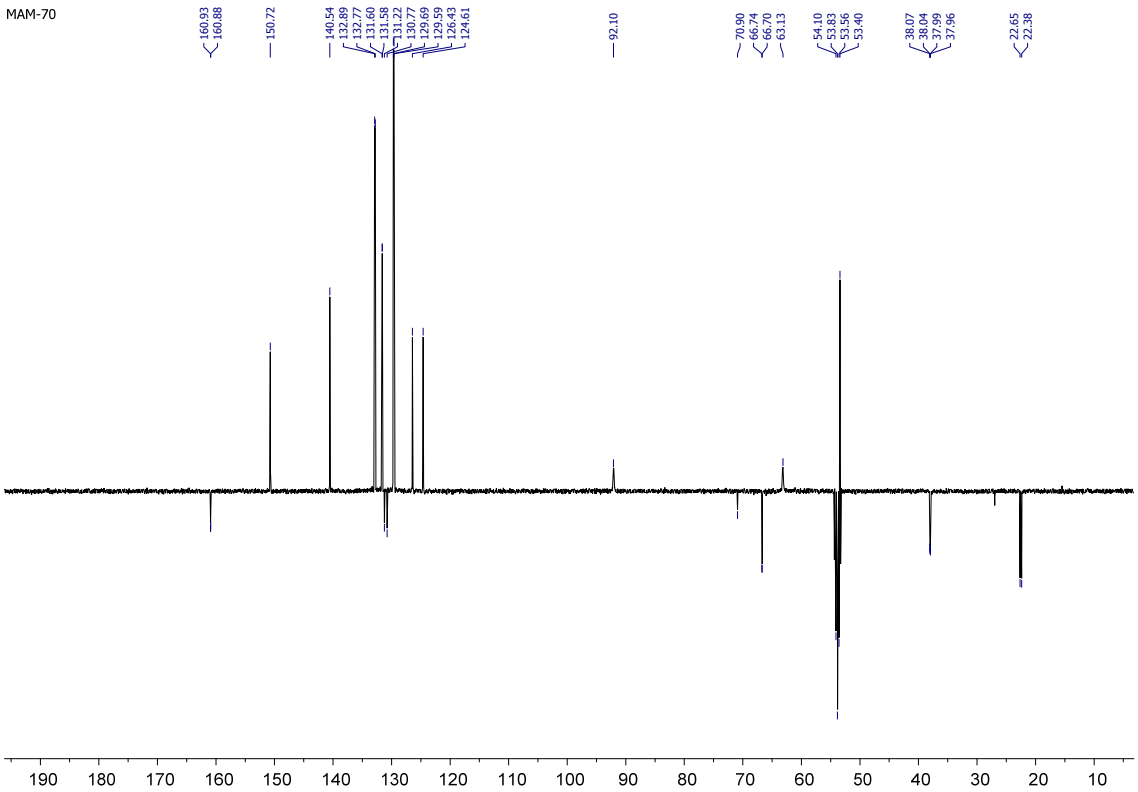

Figure S8. $^{13}C\{^{1}H\}$-apt NMR spectra of compound $[Rh(nbd)\{Ph_2(CH_2)_2Py\}]BF_4$ (**6**) in CD_2Cl_2 at 298K.

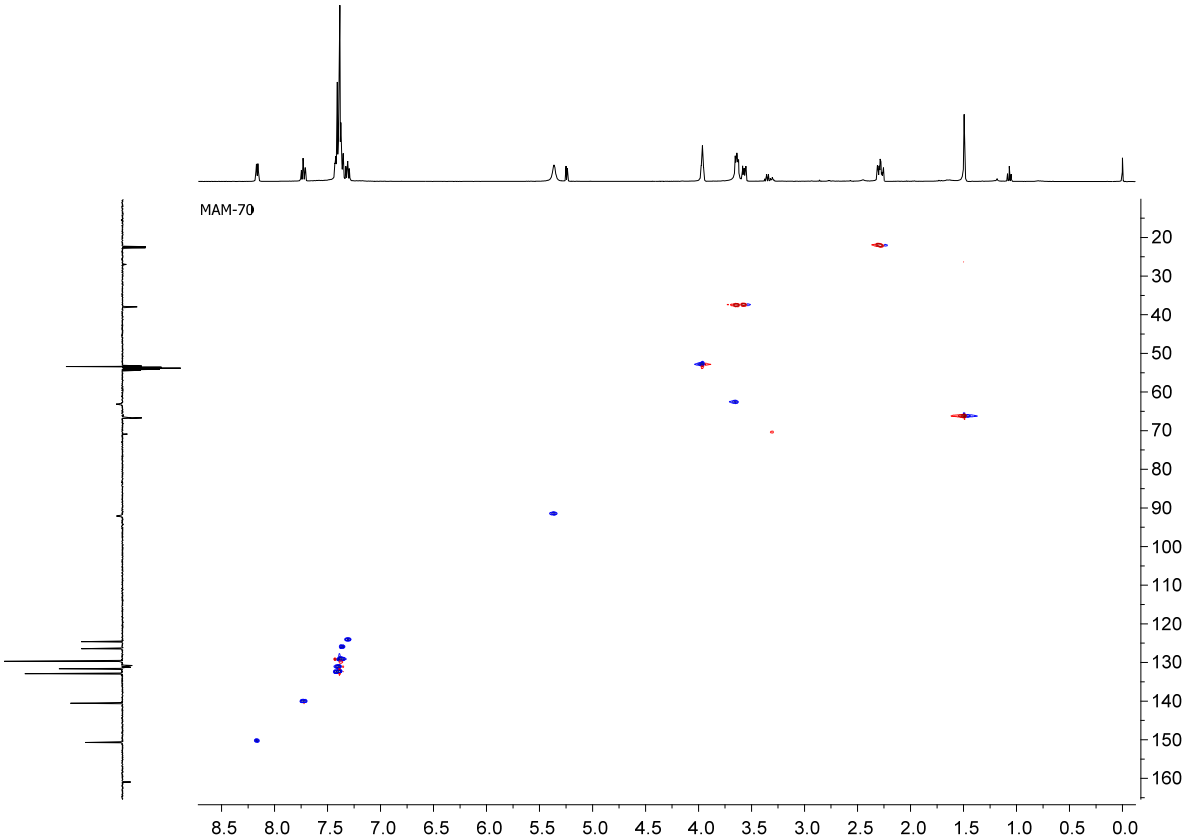

Figure S9. ^{1}H-^{13}C-HSQC NMR spectra of compound [Rh(nbd){$Ph_2(CH_2)_2Py$}]BF_4 (**6**) in CD_2Cl_2 at 298K.

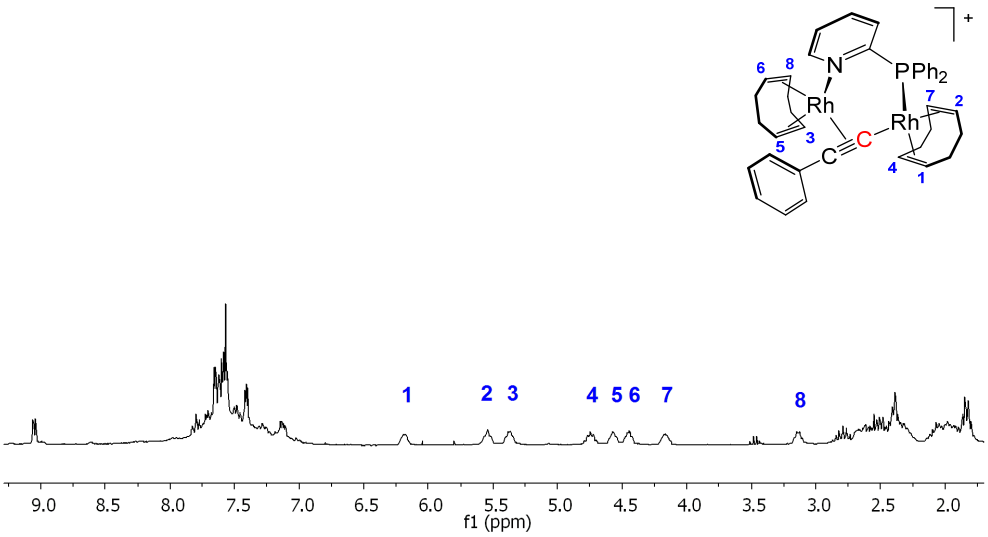

Figure S10. ^{1}H NMR spectrum of [$Rh_2(cod)_2$(μ-Ph_2PPy)(μ-C≡C-Ph)]BF_4 (**10**) in CD_2Cl_2 at 298K.

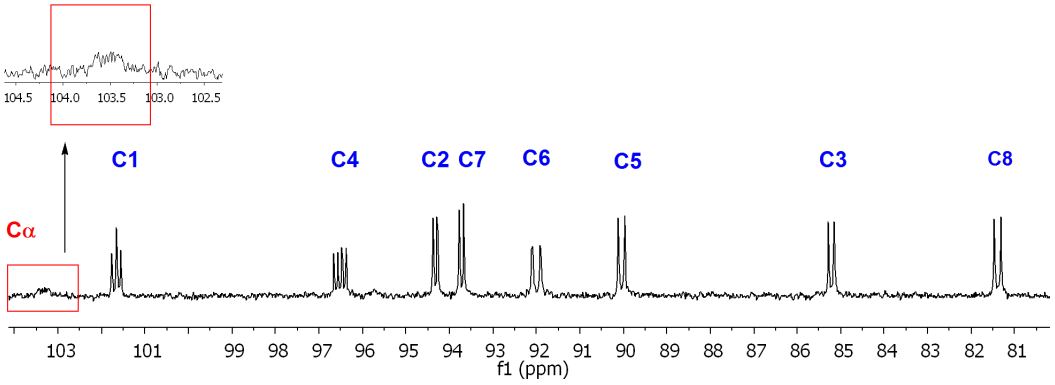

Figure S11. Selected region of the $^{13}C\{^{1}H\}$ NMR spectrum of $[Rh_2(cod)_2(\mu\text{-}Ph_2PPy)(\mu\text{-}C{\equiv}C\text{-}Ph)]BF_4$ (**10**) in CD_2Cl_2 at 298K.

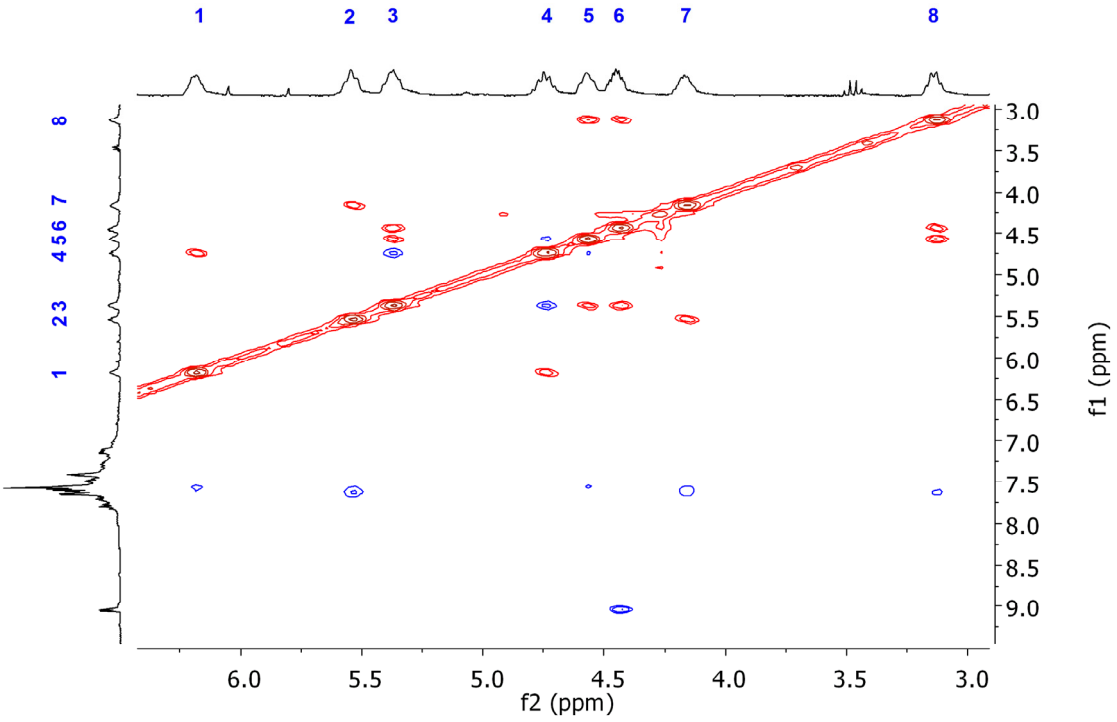

Figure S12. ^{1}H-^{1}H-NOESY NMR spectrum of $[Rh_2(cod)_2(\mu\text{-}Ph_2PPy)(\mu\text{-}C{\equiv}C\text{-}Ph)]BF_4$ (**10**) in CD_2Cl_2 at 298K.

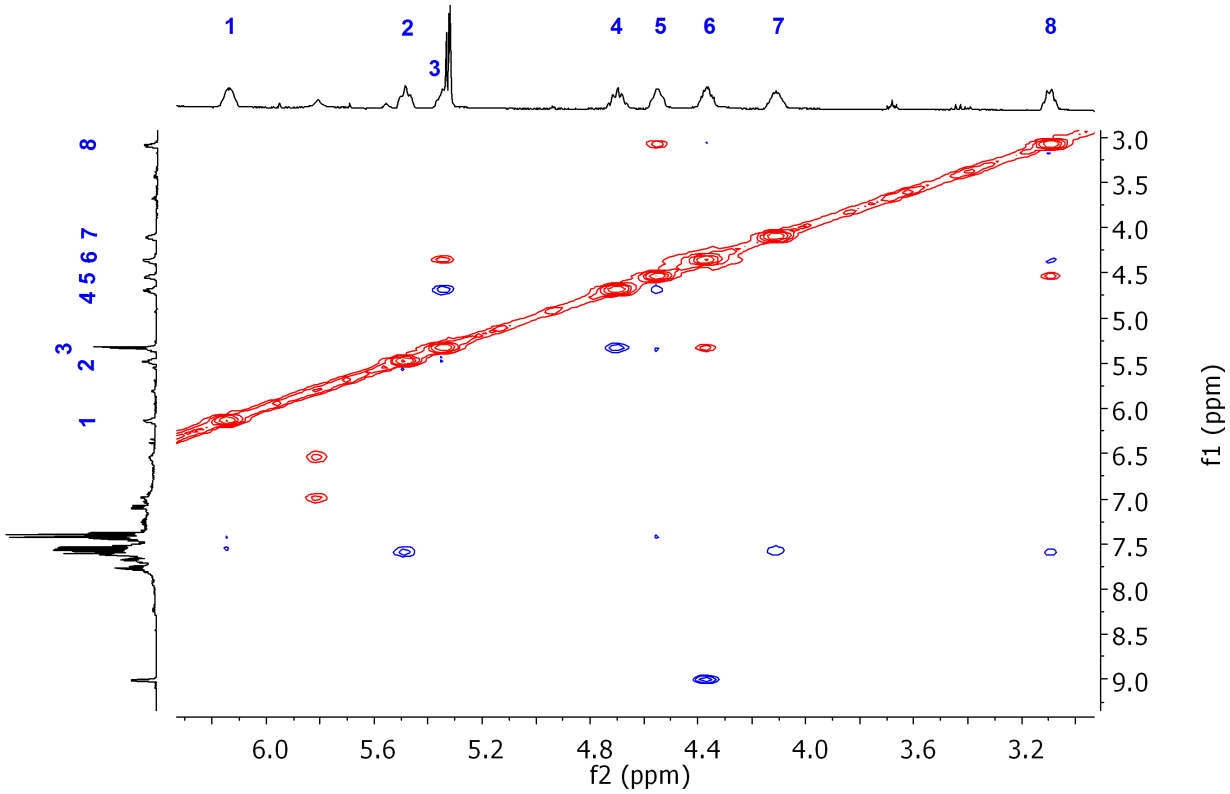

Figure S13. Selected region of the ^{1}H-^{1}H-NOESY NMR spectrum of $[Rh_2(cod)_2(\mu\text{-}Ph_2PPy)(\mu\text{-}C{\equiv}C\text{-}C_6H_5\text{-}t\text{-}Bu)]BF_4$ (**11**) in CD_2Cl_2 at 298K.

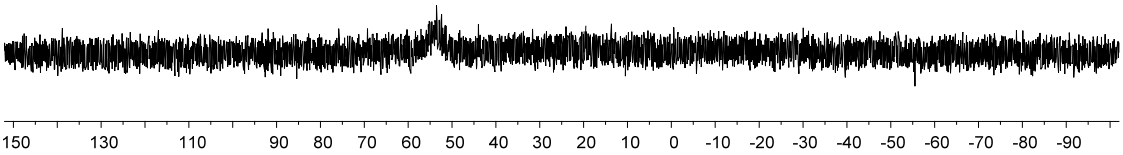

Figure S14. $^{31}P\{^{1}H\}$ NMR spectrum of compound $[Rh(Ph_2PPy)_3][BF_4]$ (**14**) in CD_2Cl_2 at 263 K.

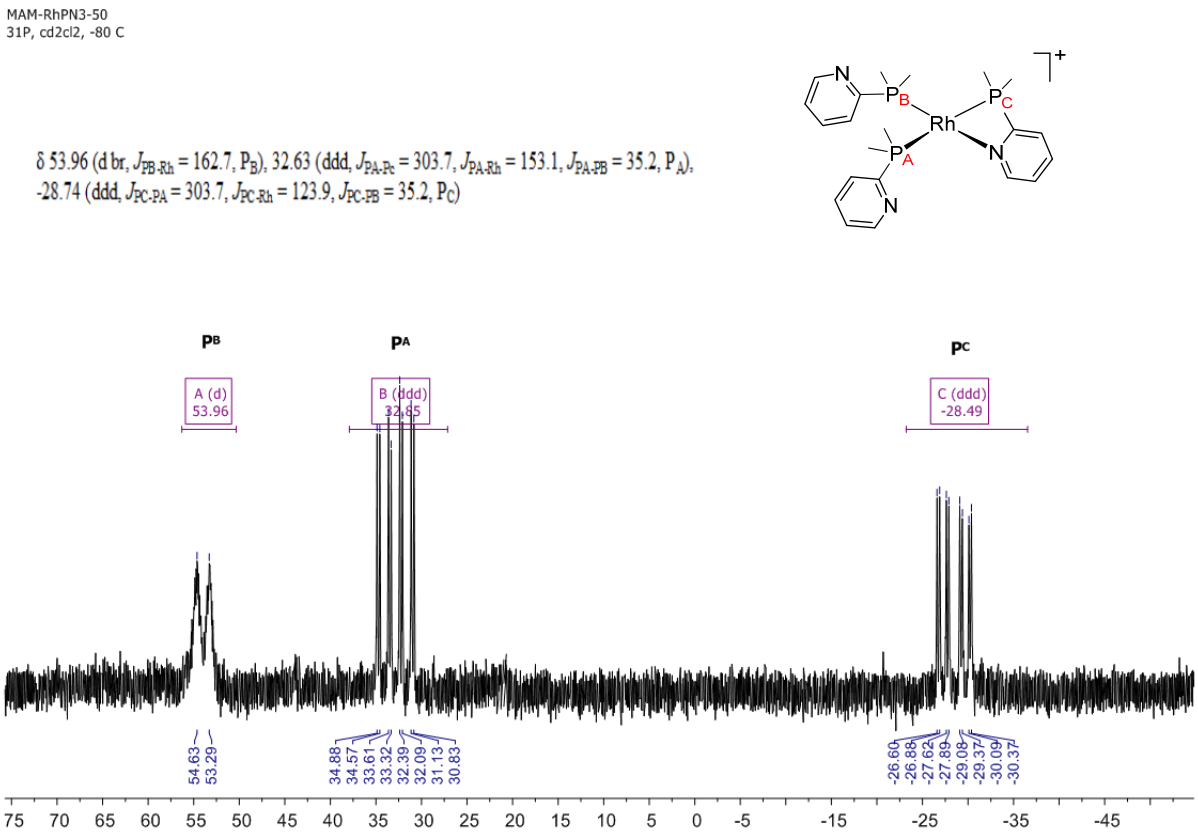

Figure S15. $^{31}P\{^1H\}$ NMR spectrum of compound $[Rh(Ph_2PPy)_3][BF_4]$ (**14**) in CD_2Cl_2 at 193 K.

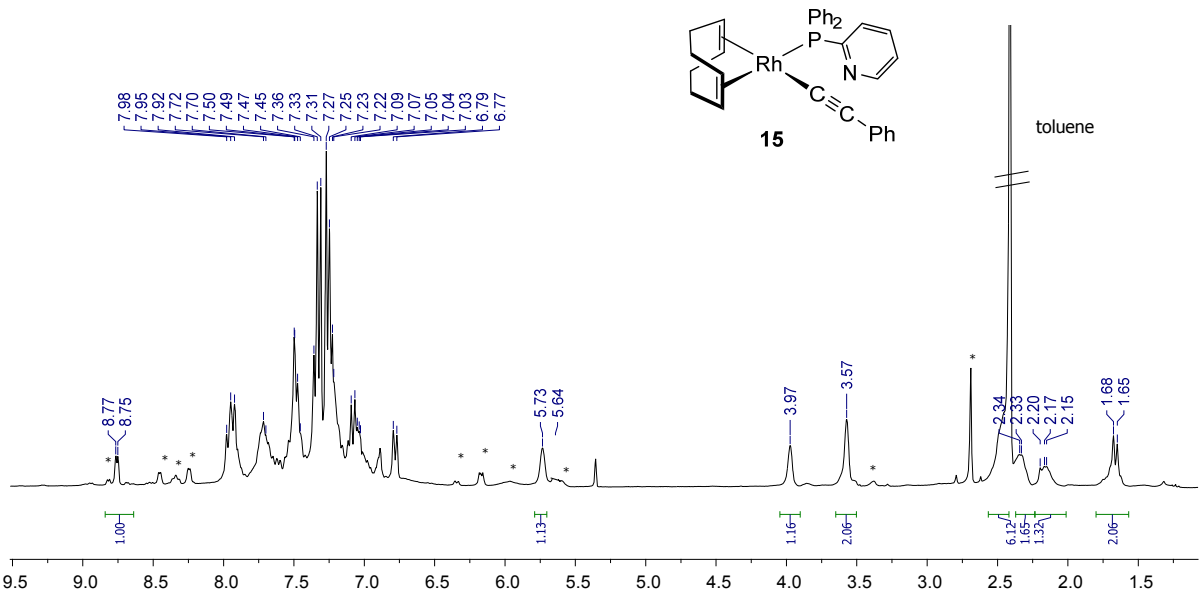

Figure S16. ^1H NMR spectrum of $[Rh(C{\equiv}C\text{-}Ph)(cod)(Ph_2PPy)]$ (**15**) (CD_2Cl_2, 220K) (* impurities).

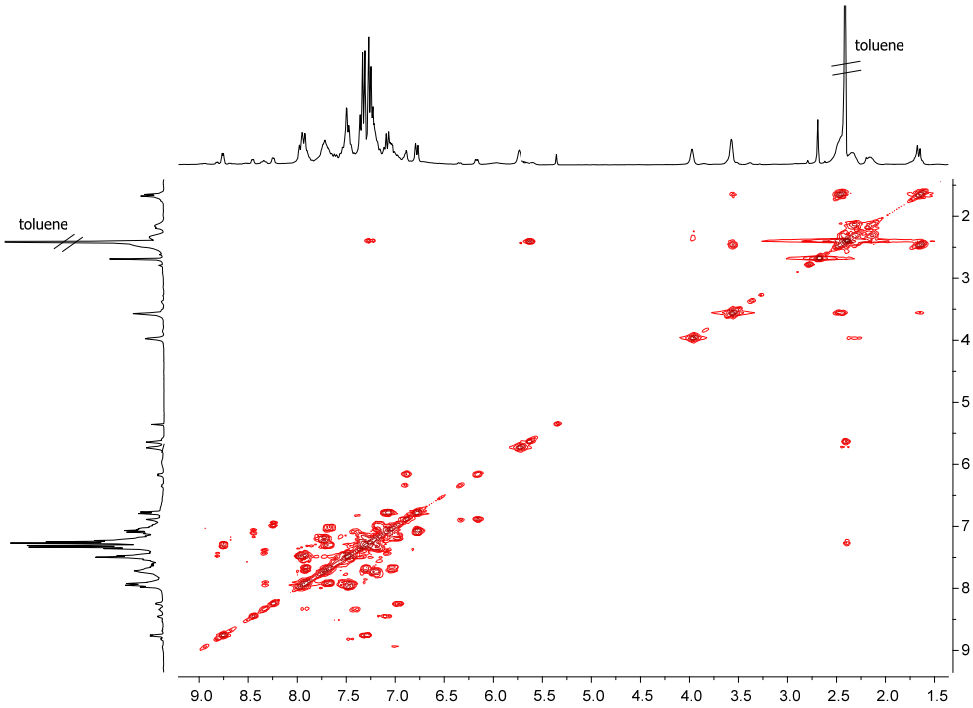

Figure S17. ^{1}H-^{1}H-COSY NMR spectrum of [Rh(C≡C-Ph)(cod)(Ph_2PPy)] (**15**) (CD_2Cl_2, 220K).

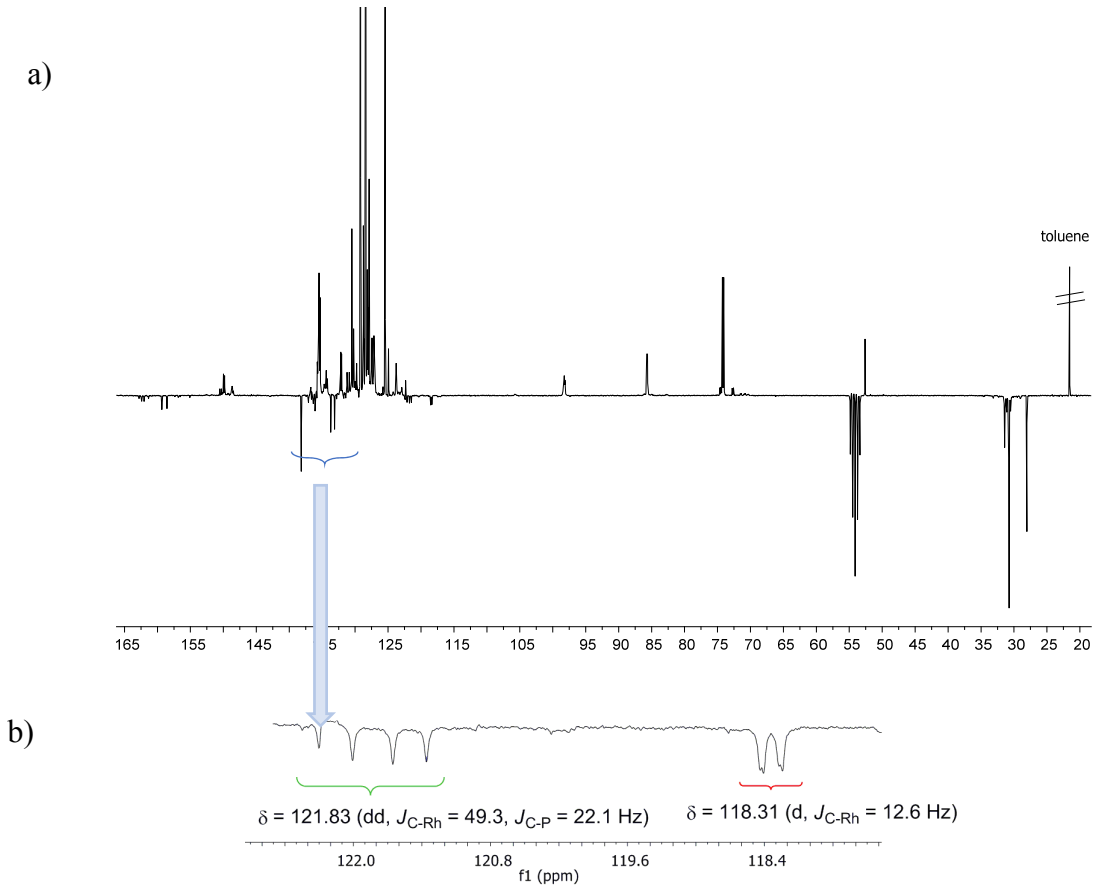

Figure S18. a) ^{13}C{^{1}H}-apt NMR spectrum of **15** in CD_2Cl_2 at 220 K. b) selected C≡C region.

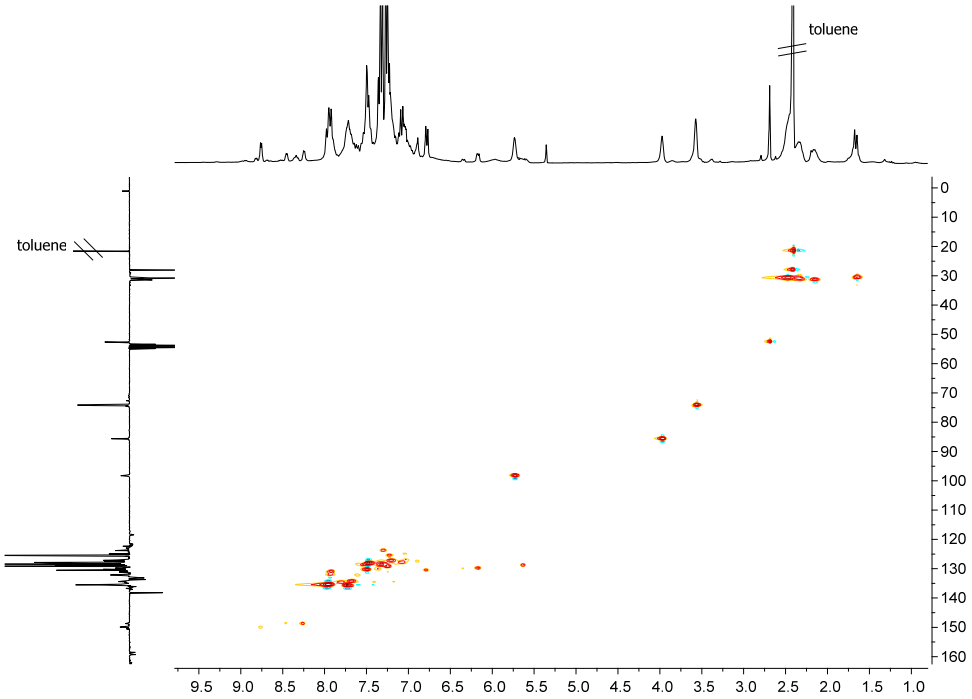

Figure S19. ^{1}H-^{13}C-HSQC NMR spectra of [Rh(C≡C-Ph)(cod)(Ph_2PPy)] (**15**) in CD_2Cl_2 at 220 K.

2.- Reaction of $[Rh(diene)(Ph_2PPy)]_n^{n+}$ with *i*PrNH$_2$.

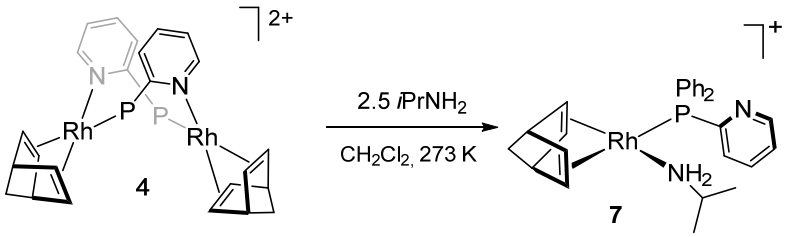

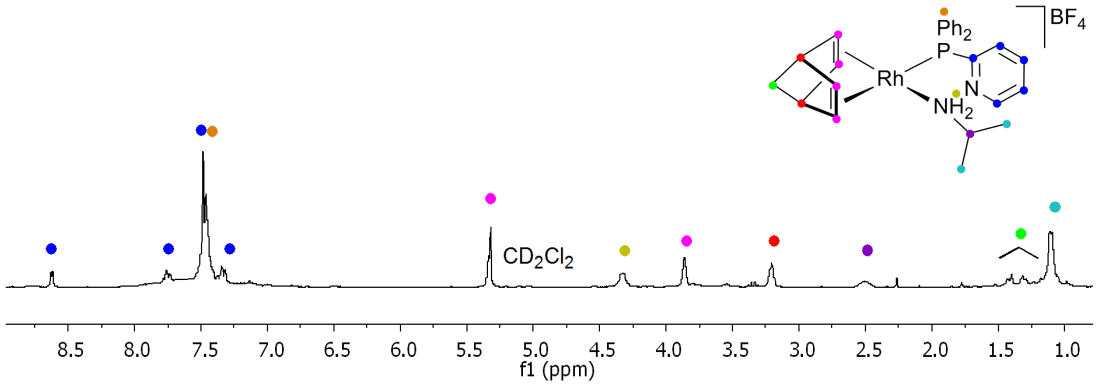

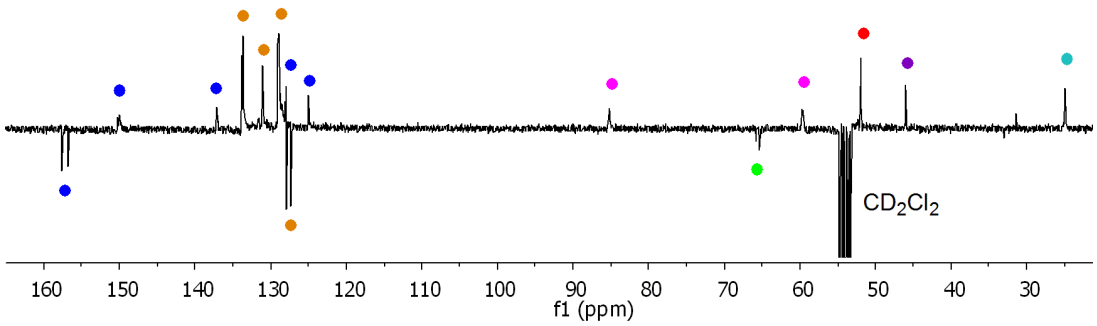

Figure S20. ^{1}H and ^{13}C{^{1}H}-apt NMR spectra of compound $[Rh(nbd)(iPrNH_2)(Ph_2PPy)][BF_4]$ (**7**) in CD_2Cl_2 at 195 K.

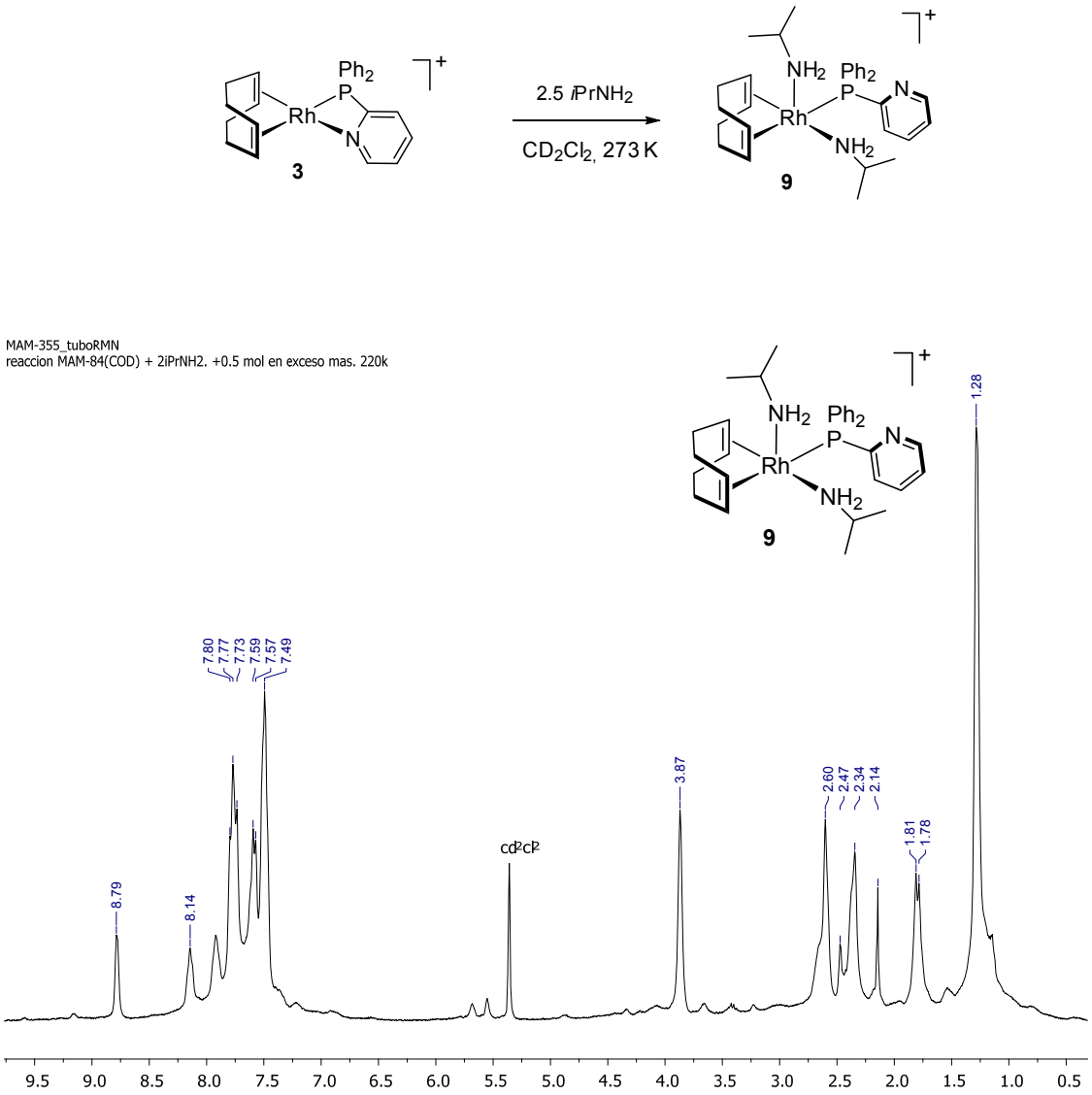

Figure S21. ^{1}H NMR spectrum of $[Rh(cod)(iPrNH_2)_2(Ph_2PPy)]^+$ (**9**) formed *in situ*, $[^iPrNH_2]$:[**3**] = 2.5 (CD_2Cl_2, 220 K).

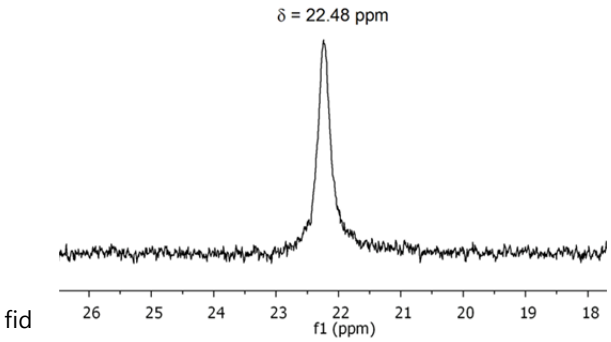

Figure S22. ^{31}P{^{1}H} NMR spectrum of $[Rh(cod)(iPrNH_2)_2(Ph_2PPy)]^+$ (**9**) formed *in situ*, $[^iPrNH_2]$:[**3**] = 2.5 (CD_2Cl_2, 220 K).

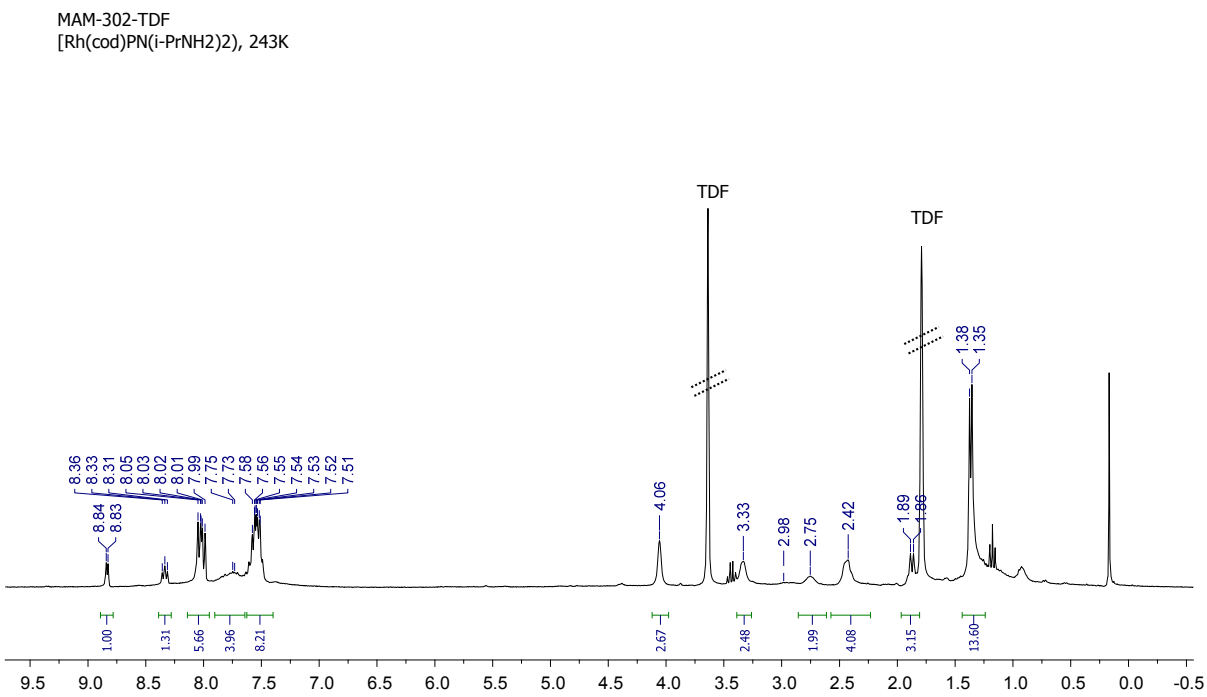

Figure S23. ^{1}H NMR spectrum of $[Rh(cod)(iPrNH_2)_2(Ph_2PPy)]^+$ (**9**) formed *in situ*, $[^{i}PrNH_2]$:[**3**] = 2.5 (THF-d_8, 243 K).

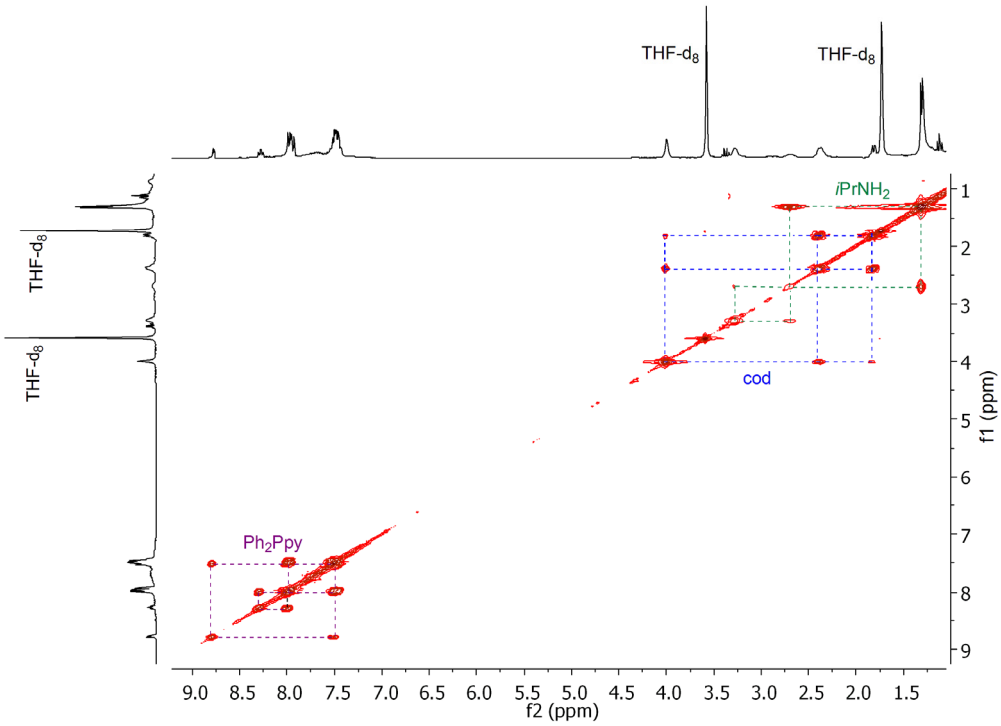

Figure S24. ^{1}H-^{1}H COSY NMR spectrum of $[Rh(cod)(iPrNH_2)_2(Ph_2PPy)]^+$ (**9**) *in situ*, $[iPrNH_2]$:[**3**] = 2.5 (THF-d_8, 243 K).

3.- Reaction of [Rh(cod)(Ph_2PPy)][BF_4] (3) with PhC≡CH in THF-d_8.

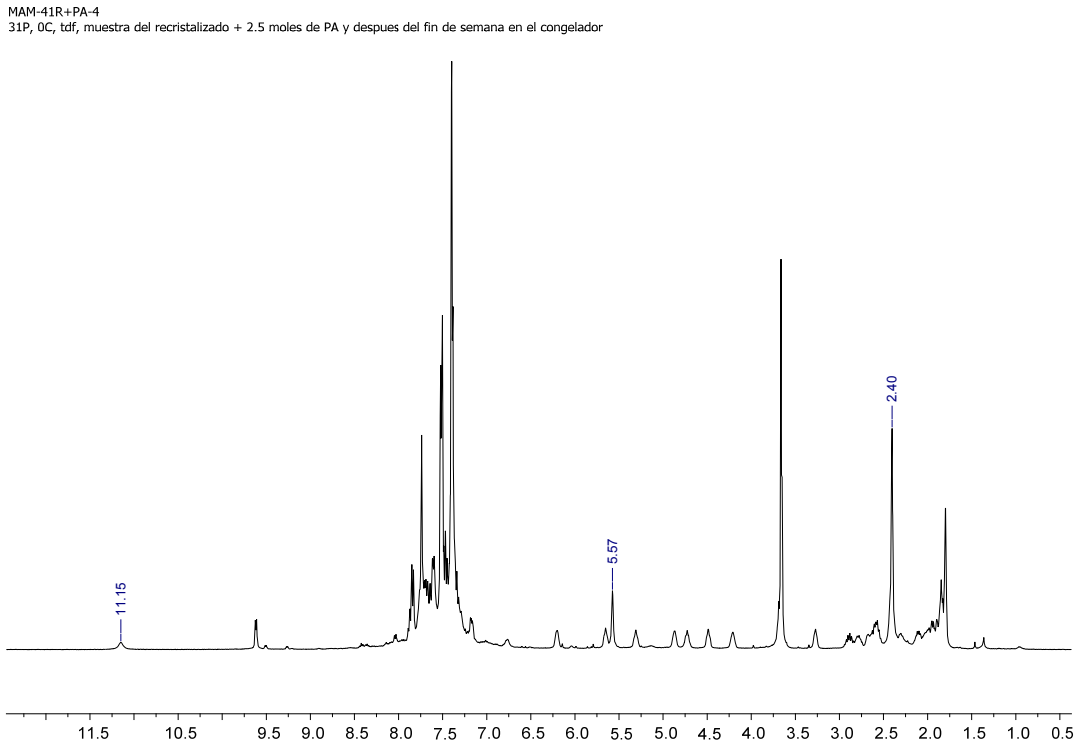

Figure S25. ^{1}H NMR spectrum of the reaction of **3** with PhC≡CH (1:2.5) in THF-d_8 at 273 K.

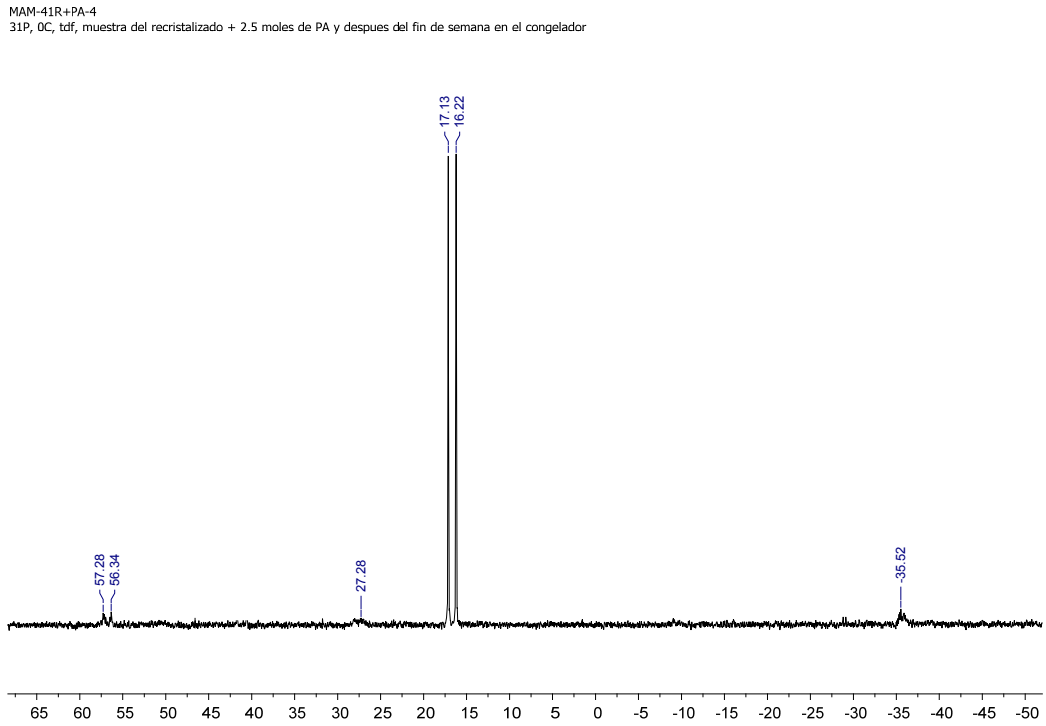

Figure S26. ^{31}P{^{1}H} NMR spectrum of the reaction of **3** with PhC≡CH (1:2.5) (THF-d_8, 273 K).

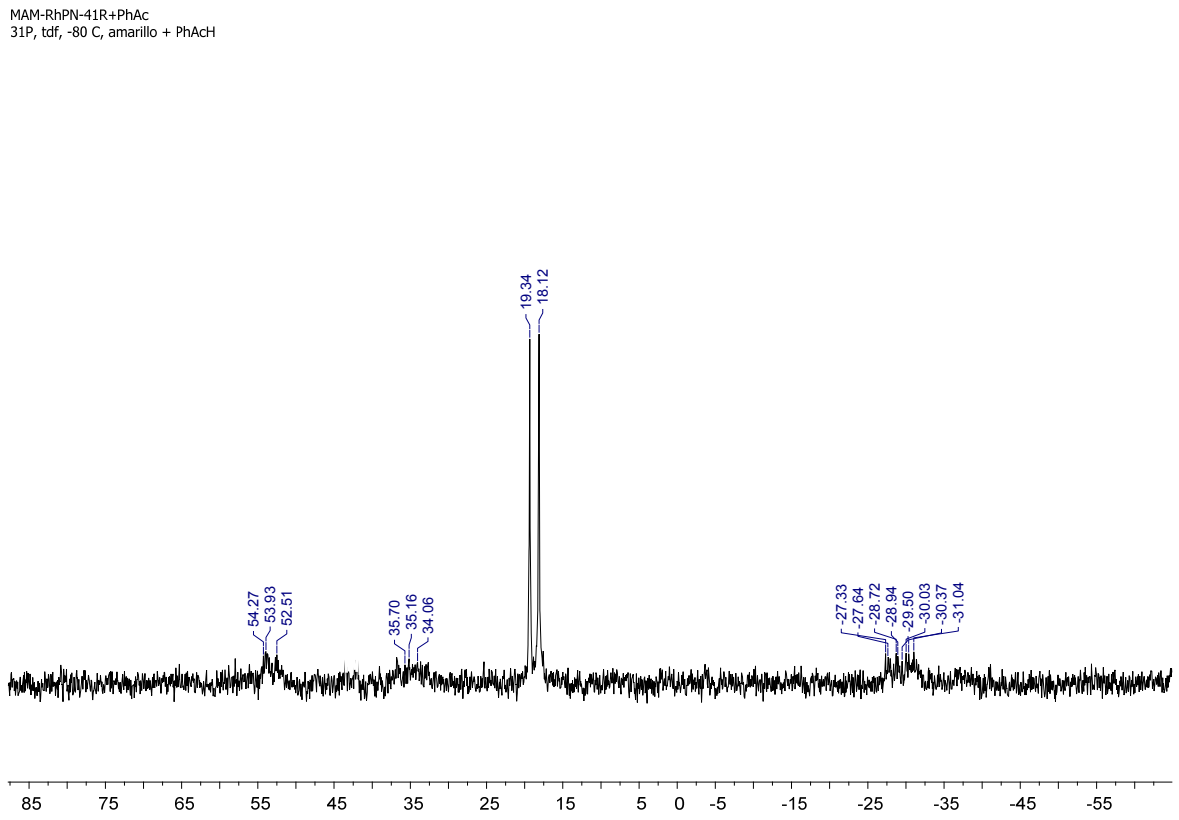

Figure S27. $^{31}P\{^{1}H\}$ NMR spectrum of the **3** with PhC≡CH (1:2.5) in THF-d_8 at 193 K.

4.- Reaction of $[Rh(cod)(Ph_2PPy)]^+$ (3) PhC≡CH in CH_2Cl_2: formation of $[(cod)Rh(Ph_2PC_5H_4N\text{-}C{=}CHPh)]BF_4$ (13).

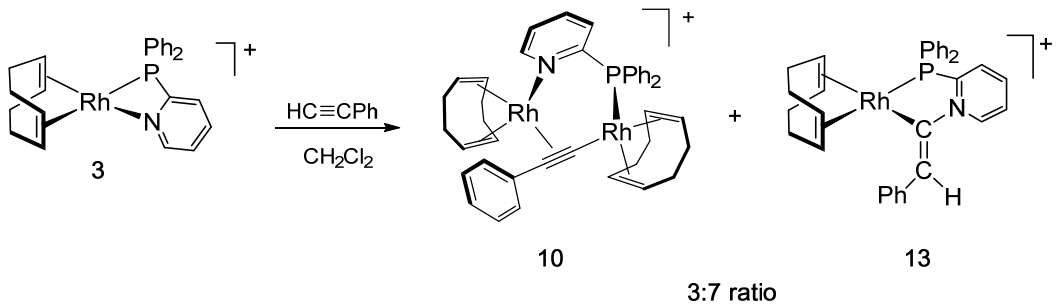

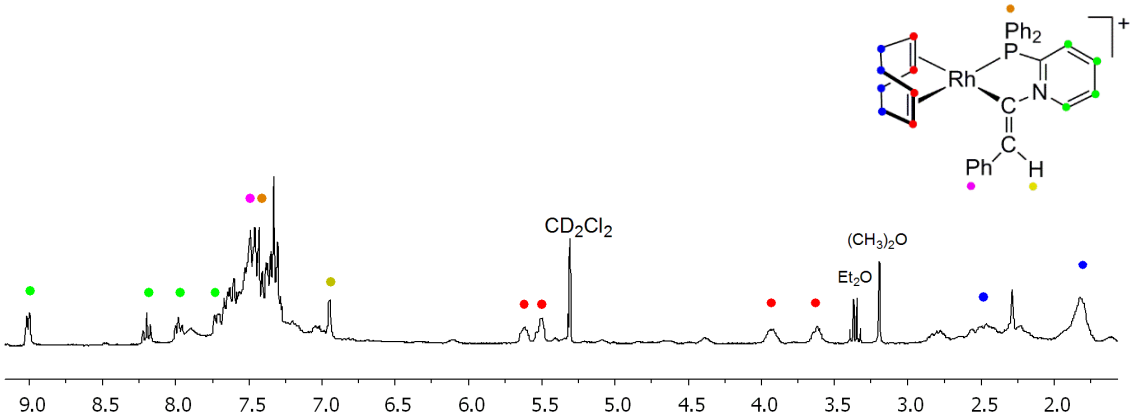

Figure S28. Resonances of **13** in the ^{1}H NMR spectrum of the **10**/**13** mixture in CD_2Cl_2 at 213 K.

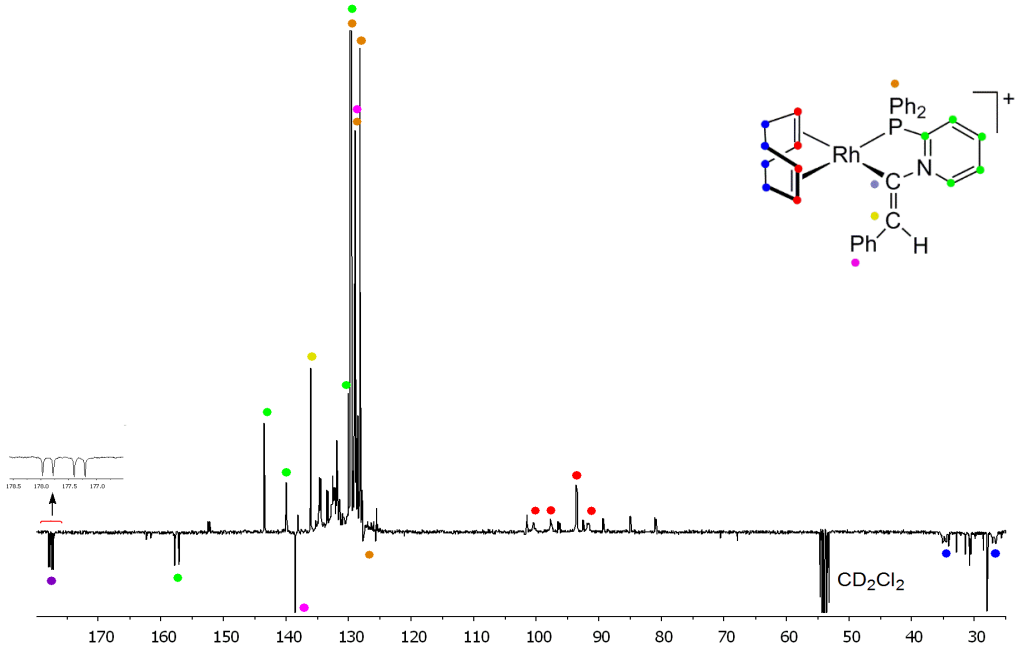

Figure S29. Resonances of **13** in the $^{13}C\{^1H\}$-apt NMR spectrum of the **10**/**13** mixture in CD_2Cl_2 at 213 K.

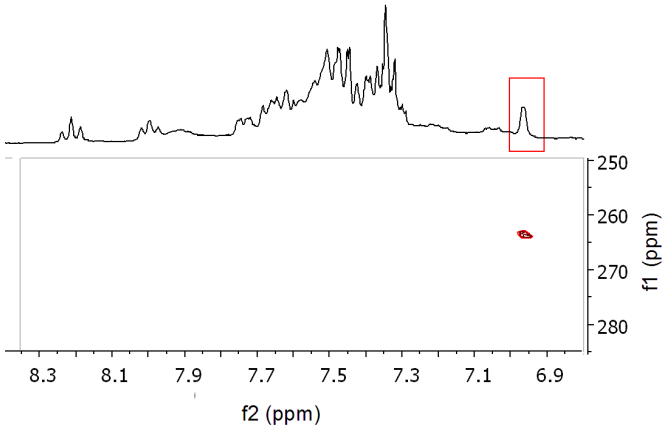

Figure S30. Selected region of the ^{1}H-^{15}N-HMQC NMR spectrum for **13** in CD_2Cl_2 at 213 K.

5.- Monitoring of the reaction of [Rh(nbd)(*i*PrNH$_2$)(Ph$_2$PPy)]BF$_4$ (7) with PhC≡CH.

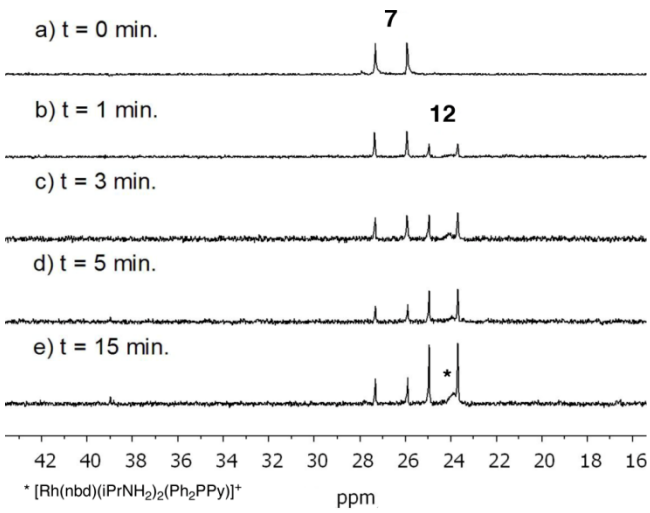

Figure S31. $^{31}P\{^{1}H\}$ of the reaction of **7** (0.022 mmol, 0.044 M) with PA (0.11 mmol, 0.22 M) by in CD_2Cl_2 at 195 K (t is the time at room temperature between spectra).

6.- Characterization of PPA samples: selected chromatograms and conformation plots.

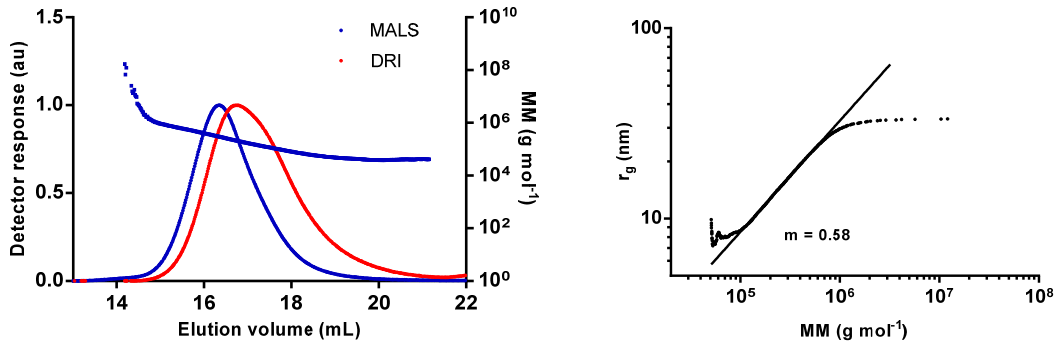

Figure S32. a) Light scattering (blue) and refractive index (red) chromatograms, MM (molar mass) vs elution volume plot for a PPA sample prepared using catalyst [RhCl(cod)(Ph_2PPy)] (**1**) in THF. b) Log-log plot of the radius of gyration (r_g) vs MM.

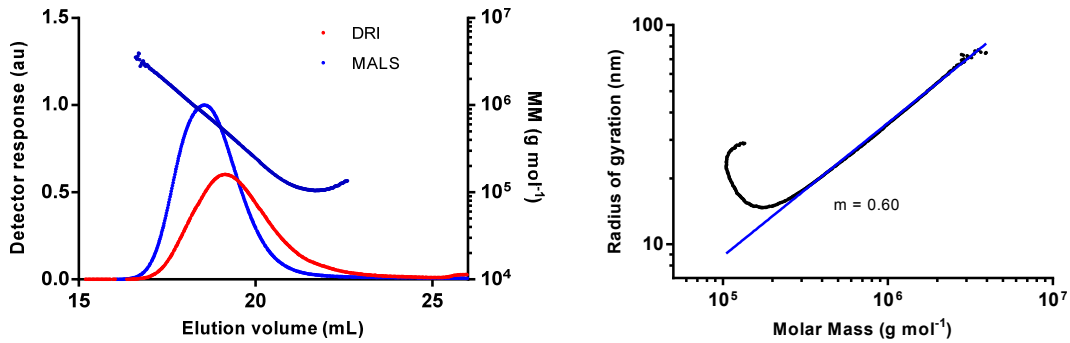

Figure S33. a) Light scattering (blue) and refractive index (red) chromatograms, MM (molar mass) vs elution volume plot for a PPA sample prepared using catalyst [RhCl(nbd)(Ph_2PPy)] (**2**) in THF. b) Log-log plot of the radius of gyration (r_g) vs MM.

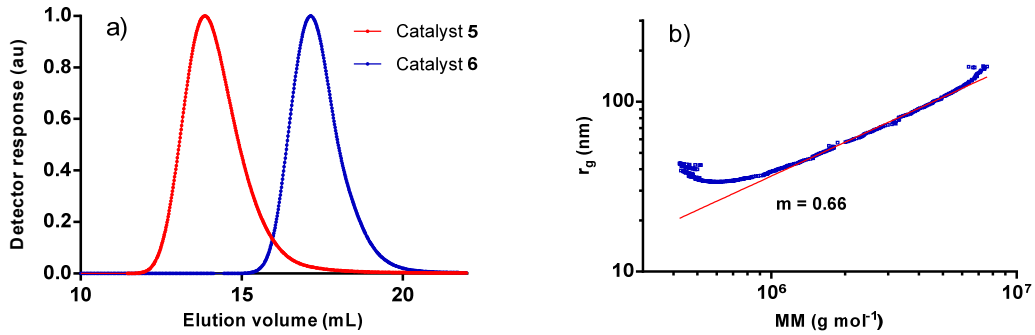

Figure 34. a) Light scattering chromatograms for PPA samples prepared using catalysts [RhCl(nbd){$Ph_2(CH_2)_2Py$}] (**5**) (red) and [Rh(nbd){$Ph_2P(CH_2)_2Py$}][BF_4] (**6**) (blue) in THF. b) Log-log plot of the radius of gyration (r_g) vs MM for the sample prepared with catalyst [RhCl(nbd){$Ph_2(CH_2)_2Py$}] (**5**).

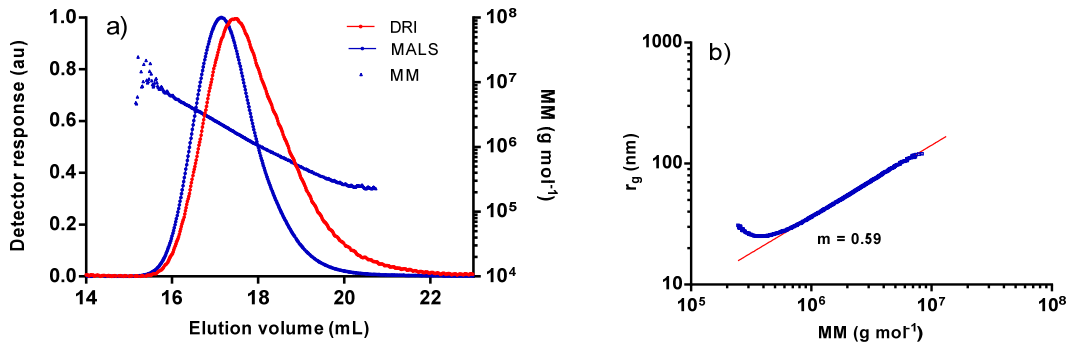

Figure S35. a) Light scattering (blue) and refractive index (red) chromatograms, MM (molar mass) vs elution volume plot for a PPA sample prepared using catalyst [Rh(nbd){$Ph_2P(CH_2)_2Py$}][BF_4] (**6**) in THF. b) Log-log plot of the radius of gyration (r_g) vs MM.

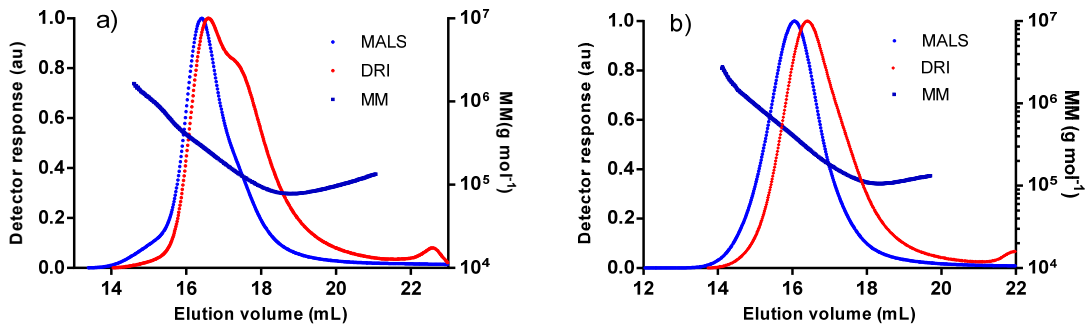

Figure S36. a) Light scattering (blue) and refractive index (red) chromatograms, MM (molar mass) vs elution volume plot for a PPA sample prepared in THF using: a) [Rh(nbd)(μ-Ph_2PPy)]$_2$[BF_4]$_2$ (**4**) + *i*$PrNH_2$, and b) [Rh(nbd)(*i*$PrNH_2$)(Ph_2PPy)]BF_4 (**7**).

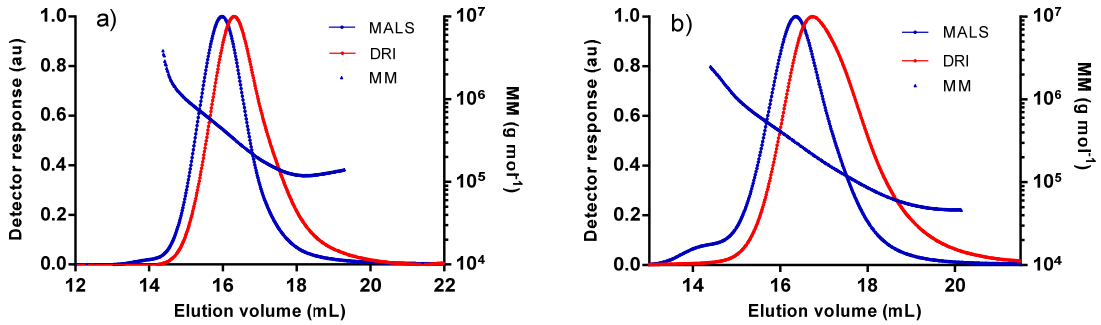

Figure S37. a) Light scattering (blue) and refractive index (red) chromatograms, and MM (molar mass) vs elution volume plot for a PPA sample prepared using: a) [Rh(cod)(Ph_2PPy)][BF_4] (**3**) + *i*$PrNH_2$, and b) [Rh(C≡CPh)(cod)(Ph_2PPy)] (**15**).

7.- DFT calculations.

Table S1. DFT Calculated energies (Hartree).

Compound	E (Hartree)	G (Hartree)
comp3	-1473,946973	-1473,55531
comp3_dimer	-2947,893322	-2947,07217
comp4	-2866,760676	-2866,042813
comp4_monomer	-1433,3762	-1433,033767
comp13	-1782,425403	-1781,928647
compA	-1782,39875	-1781,904294
compB	-1782,397789	-1781,903075
TS_b_c	-1782,381049	-1781,893859
compC	-1782,392764	-1781,897724
TS_c_d	-1782,374933	-1781,882224
compD	-1782,384944	-1781,891898
phenylacetylene	-308,4211262	-308,34198